



The porous media model for the hydraulic system of a conifer tree: Linking sap flux data to transpiration rate

Yao-Li Chuang^{a,b,*}, Ram Oren^c, Andrea L. Bertozzi^{a,b,d},
Nathan Phillips^e, Gabriel G. Katul^{c,f}

^a Department of Physics, Duke University, Physics Bldg., Science Dr. Box 90305, Durham, NC 27708-0305, USA

^b Department of Mathematics, University of California Los Angeles, 405 Hilgard Avenue, Los Angeles, CA 90095-1555, USA

^c Nicholas School of the Environment and Earth Sciences, Box 90328, Duke University, Durham, NC 27708-0328, USA

^d Department of Mathematics, Duke University, Physics Bldg., Science Dr. Box 90320, Durham, NC 27708-0320, USA

^e Department of Geography, Boston University, Boston, MA 02215, USA

^f Department of Civil and Environmental Engineering, Duke University, Durham, NC 27708, USA

Received 9 February 2004; received in revised form 25 February 2005; accepted 28 March 2005

Available online 2 August 2005

Abstract

Linking sap flow in tree boles to plant transpiration continues to be a fundamental and practical research problem in physiological ecology and forest hydrology. Many models have been proposed to describe water movement within trees with varying degrees of success. The prevailing resistance–capacitance (*RC*)-circuit models have the advantage of being easy to implement. However, *RC* models are ordinary differential equation (ODE) models that reduce the spatial–temporal dynamics of a tree hydraulic system to the temporal variation of simplified quantities; thus, the *RC* parameterization is more empirical and open to various interpretations. For coniferous trees, a reasonable alternative to *RC* circuit models is a porous media (PM) model, which is a partial differential equation (PDE) model that describes the spatial–temporal dynamics. The model more closely represents the physical elements of the conifer hydraulic system but also requires a direct estimation of its properties. Our proposed PM model is original in that it formulates a theoretical link between measured quantities (i.e., sap flux density and tree structure) and model parameters, obtained during nighttime, which permits direct numerical conversion of sap flow to transpiration rate during daytime. In addition to fully simulating the PDE, we propose an alternative method to transform the PDE into a set of ODEs, to significantly reduce computational demands. Although the ODE results are noisy, the transpiration pattern produced by the ODE, once filtered, is similar to that of the PDE. We demonstrate that measurements of the sap flux in multiple positions below and within the crown can be used to compute the height-dependent transpiration rate; but if rates of bulk crown transpiration are of primary interest, readily obtainable measurements at two heights, at the base of the tree and below the crown, are sufficient for the computation.

© 2005 Elsevier B.V. All rights reserved.

Keywords: Hydraulic system; Porous media; Sap flux; Transpiration; Xylem; Conifers

* Corresponding author.

E-mail address: chuang@phy.duke.edu (Y.-L. Chuang).

Nomenclature

A	cross section area (m^2)
A_0	base cross section area (m^2)
b_0	a proportional constant (kg m^{-3})
b_1	a proportional constant (kg m^{-3})
c	hydraulic capacitance ($\text{m}^{-2} \text{s}^2$)
c_2	vulnerability parameter 1
C	capacitance of circuit model ($\text{m}^{-2} \text{s}^{-1}$)
d	vulnerability parameter 2 ($\text{kg m}^{-1} \text{s}^{-2}$ (=Pa))
E	transpiration rate ($\text{kg m}^{-2} \text{s}^{-1}$)
E_a	actual transpiration rate ($\text{kg m}^{-2} \text{s}^{-1}$)
E_{new}	corrected transpiration rate ($\text{kg m}^{-2} \text{s}^{-1}$)
g	gravitational acceleration (m s^{-2})
g_s	stomatal conductance ($\text{m}^{-1} \text{s}$)
H	total height of the tree (m)
J	water flux ($\text{kg m}^{-2} \text{s}^{-1}$)
J_e	exp. measured water flux ($\text{kg m}^{-2} \text{s}^{-1}$)
\hat{J}	water flow (kg s^{-1})
K	xylem conductance (s)
K_{max}	max. xylem conductance (s)
\hat{K}	xylem conductivity ($\text{m}^2 \text{s}$)
\hat{K}_{max}	max. xylem conductivity ($\text{m}^2 \text{s}$)
l	leaf area per unit length (m)
P	power of retention curve
R	resistance of circuit model ($\text{m}^{-1} \text{s}^{-1}$)
R_g	global radiation (kg s^{-3} (=W m^{-2}))
S	a sink term (kg s^{-1})
t	time (s)
T	relaxation time constant (s^{-1})
x	position (m)
x_H	a relative higher position (m)
x_L	a relative lower position (m)

Greek letters

α	taper rate (m^{-1})
Φ	hydrostatic pressure ($\text{kg m}^{-1} \text{s}^{-2}$ (=Pa))
Φ_0	retention potential coeff. ($\text{kg m}^{-1} \text{s}^{-2}$ (=Pa))
η	a suitable time interval (s)
κ	saturated K/c ($\text{m}^2 \text{s}^{-1}$)
θ	xylem moisture content (kg m^{-3})
θ_0	steady state solution of θ (kg m^{-3})
θ_{sat}	saturated θ (kg m^{-3})

$\tilde{\theta}$	small perturbation of θ (kg m^{-3})
Θ	total moisture content (kg)
Ξ	total transpiration rate (kg s^{-1})
ρ	water density (kg m^{-3})
Ψ	total water potential ($\text{kg m}^{-1} \text{s}^{-2}$ (=Pa))

1. Introduction

Measuring and modeling transpiration rates and bulk canopy conductance is a fundamental and practical problem in studies on tree physiology, forest ecology and hydrology and biosphere–atmosphere exchange processes. Stomata play a dominant role in controlling CO_2 uptake and partitioning of net radiation between latent and sensible heat flux (Verhoef and Allen, 2000; Tanaka, 2002; Zhan et al., 2003). Thus, biosphere–atmosphere flux measurement networks and free air CO_2 enrichment (FACE) experiments require a quantitative response of bulk stomatal conductance to variables such as light, vapor pressure deficit and soil moisture, or to the increase in elevated atmospheric CO_2 (Baldocchi and Meyers, 1998; Lai et al., 2000; Schäfer et al., 2003). However, tree transpiration, used in calculating bulk or mean canopy stomatal conductance, is difficult to measure and is commonly inferred from sap flow measurements (Marshall, 1958; Swanson and Whitfield, 1981; Granier, 1985; Granier et al., 1990; Čermák et al., 1995; Oren et al., 1998).

Calculating transpiration from sap flux has its own share of theoretical and practical problems. For example, the ability of tall trees to store water results in a lag between sap flux and transpiration rate (Waring et al., 1979; Jarvis et al., 1981; Goldstein et al., 1984, 1998; Hunt and Nobel, 1987; Hunt et al., 1991; Loustau et al., 1996, 1998; Phillips et al., 1999, 2004). This lag is the main motivation for modeling trees with resistance–capacitance (RC)-circuits. There are many variants of the RC model with different degree of complexity (Cowan, 1965; Slatyer, 1967; Lang et al., 1969; Cowan, 1972; Hunt et al., 1991; Jones, 1992, pp. 72–105; Phillips et al., 1997; Loustau et al., 1998). These models can always be reduced to a simplified RC circuit model, where R is the resistance of xylem conduits and C is the capacitance of water storage (Fig. 1a). The models are used to estimate an effective R and C

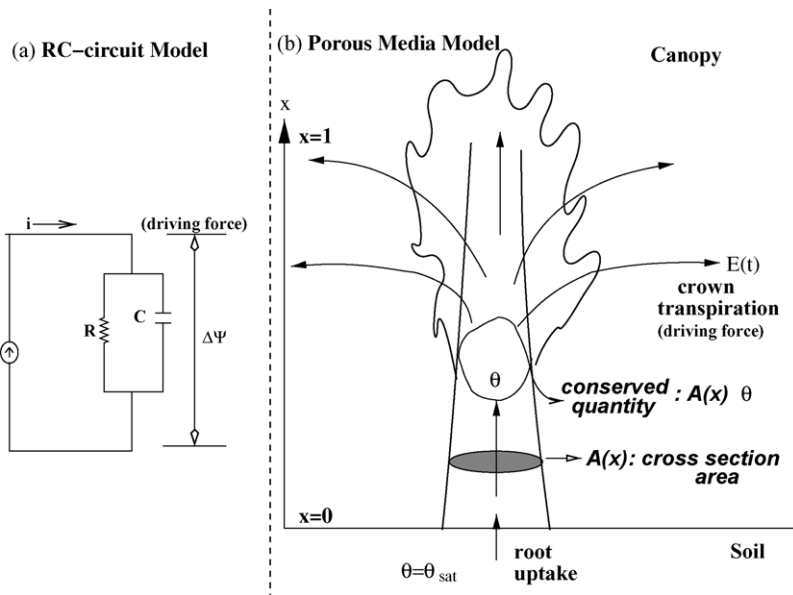


Fig. 1. (a) The simplest RC circuit model commonly used to link sap flow and transpiration. R is the resistance of the xylem; C represents the water storage inside the tree; the sap flow is i , driven by the water potential difference $\Delta\Psi$. (b) A schematic representation of the porous media model showing the xylem moisture content $\theta = \theta(x, t)$ as the conserved quantity. The plant hydraulic problem is treated as one-dimensional for simplicity, and therefore, $x = 0$ represents the base of the trunk while $x = 1$ is for the top of the crown. The lower boundary condition is controlled by soil moisture content, which is assumed saturated. The upper boundary condition is no flux at crown top. The crown transpiration $E(t)$ is treated as a driving force while combining the continuity equation with Darcy's law.

to calculate the time lag. The RC constant can be used to adjust for the time lag between sap flux and transpiration in the calculation of stomatal conductance (e.g., Phillips et al., 1997; Loustau et al., 1998). A simpler and thus commonly used method to partially account for the time lag is to artificially shift sap flux time series so as to maximize its correlation with the vapor pressure deficit (VPD, kPa) or radiation (R_g , $W\ m^{-2}$) time series (Oren et al., 1999; Phillips et al., 1999). Such analysis assumes that VPD or R_g is synchronized with canopy transpiration, and does not adjust for the attenuation of the sap flux signal due to storage effects.

The sap flux is inherently more attenuated than the real transpiration because water storage within the tree system functions as a low-pass filter. As a result, the additional variation in transpiration is distributed to a relative later time in the diurnal pattern of sap flux. This extra water flux is often discarded due to inherent difficulties of modeling redistribution of water, which results in a net loss of real transpiration, and an underestimate of mean canopy stomatal conductance during

certain times of the day (Phillips and Oren, 1998; Ewers and Oren, 2000). One solution to both problems of time lag and signal attenuation is to fully simulate all RC organ components explicitly rather than just calculating the effective RC constant (Hunt et al., 1991). This approach ensures that none of the water flowing into the tree is neglected. However, the RC circuit representation often yields an ordinary differential equation (ODE), which reduces the spatial-temporal dynamics of a tree hydraulic system to the temporal variation of several simplified artificial components; thus, specifying the RC component of each organ is difficult at best and impractical to measure. Additionally, the capacitance of a typical RC circuit recharges when the voltage (potential difference) is applied and discharges when the voltage is removed; this does not exactly reflect the dynamic behaviors of the tree hydraulic storage which is refilled at night when water potential difference decreases and drained during the day when water potential difference increases. Another problem with general RC circuit models is that the moisture content,

unlike electrical charges, can only be non-negative. The linear capacitance in RC circuit models does not prevent the moisture content from going negative and thus allows unlimited water withdrawal.

We explore an alternative solution, a porous media (PM) model, based on the finding that conifer xylem can be treated as such medium because it is composed of tracheids (Schulte and Costa, 1996; Früh and Kurth, 1999; Kumagai, 2001; Aumann and Ford, 2002a). The PM model combines the continuity equation with Darcy's law modified to include all sinks due to transpiration. This approach leads to a mass-conserving partial differential equation (PDE) that describes the spatial–temporal dynamics of a tree hydraulic system. It also connects sap flux to transpiration without artificial water loss due to calculation. While the RC circuit models allow unlimited water withdrawal from the tree, the maximum principle guarantees that the moisture content in the PM model is bounded between a saturation point and zero; as a result, the amount of water withdrawn can never leave the moisture content lower than the values found under very dry soils and high VPD in realistic cases. Although it is conceivable that at any particular time, an RC circuit can approximate the solution of a porous medium PDE, this comes at the expense of introducing time-dependent resistors and capacitors. In most previous studies, porous media models are used for qualitative comparison (e.g., Schulte and Costa, 1996; Früh and Kurth, 1999; Aumann and Ford, 2002a). The one exception (Kumagai, 2001) requires that stomatal conductance is explicitly modeled and thus introduces additional complexity and uncertainty to the parameters. Furthermore, that model predicts water potential, a variable used for a quasi-quantitative verification of the results but not readily obtainable at high temporal and spatial density in field experiments. Building upon these previous studies, we propose a model driven by transpiration rate (Fig. 1b), rather than VPD (Fig. 1a), thereby eliminating the need for a separate stomatal conductance model. Because we use sap flux measured at the base of the tree and we set the boundary condition at the soil surface, the model is useful for above ground plant hydraulics only. Xylem moisture content is chosen as our state variable and is the conserved quantity of the PDE. We also derive an expression for sap flux based on xylem moisture content for direct comparison with field measurements.

As a case study, we use data obtained from a Norway spruce (*Picea abies* L.) forest experiment (Phillips et al., 2001, 2004). For this experiment, the tree was confined to a chamber that can be flushed in order to create a sudden VPD drop as a perturbation. Phillips et al. (2004) used the perturbed sap flux data to capture the hydraulic characteristics of the tree by applying the Laplace transform to the RC circuit model. In our study, the unperturbed sap flux data are used instead. The primary reasons for using the PM model are: (1) that it correctly captures the lag between transpiration and sap flux and (2) that it preserves the total mass without losing sap flux due to calculation.

The dynamics of non-linear PDEs have long been introduced to study various ecological models (Pielke et al., 1993; Cushing et al., 1996; Patten, 1997). Our PM model is such an example. By applying linear stability analysis, we show that the hydraulic characteristics of the tree can be inferred from a subset of unperturbed sap flux data collected at night, when no transpiration occurs. We show that measurements of the sap flux at several positions below and within the crown can be used to compute the height-dependent transpiration rate. Moreover, sap flux measurements at two heights, the base of the tree and below the crown, are sufficient to capture the diurnal pattern of bulk crown transpiration. Our analysis suggests that the PM model can be applied to estimate transpiration from sap flux in field experiments without artificial control or perturbations of the surrounding environment.

2. Methods

The experiment setting is briefly described. The derivation of the PM model equations as well as the boundary conditions are presented next, followed by linear stability analysis that permits us to estimate the hydraulic properties for the model from nighttime data. We then describe the full parameterization of the model and apply the model to sap flux data from a field experiment.

2.1. Setting

In this case study, we use experiment data collected in Flakaliden, Sweden on a Norway spruce tree from June 11 to July 23, 1996 (Phillips et al., 2001, 2004)

to explore the application of the PM model and compare it with the RC model calculations (Phillips et al., 2004). In this study, we used an ensemble average of diurnal values from 20 days in which complete data were available.

Sap flux was measured using a Granier-type constant heat dissipation probe (Granier, 1985) positioned in the outer 20 mm of the hydroactive xylem of a 6.7 m tall tree in a closed-top chamber. Because the crown extended nearly to the tree base, it is assumed that the entire cross section of the xylem was developed under the influence of the crown and is thus made entirely of juvenile wood without radial pattern (Phillips et al., 1996). This is supported by other direct estimates of sap flux at different radial depths at this site (Phillips et al., 2001). Measurements of the flux in the outer xylem are sufficient to estimate the flux through the entire cross section area. There were five measurement points on the subject Norway spruce tree, identified as the fraction of the measurement height (Z) over total tree height ($H=6.7$ m): (1) $Z/H=0.03$ at 0.2 m above ground; (2) $Z/H=0.16$ at 1.1 m; (3) $Z/H=0.27$ at 1.8 m; (4) $Z/H=0.54$ at 3.6 m; (5) $Z/H=0.72$ at 4.8 m. Temperature and relative humidity were measured inside the chamber and used in the calculations of vapor pressure deficit (VPD). Global radiation (R_g) was measured outside the chamber at a top of a nearby mast. All sensors were interrogated every 5 s and the half-hour average was recorded in a data logger. See Phillips et al. (2004) for complete details on instruments, ancillary data and measurement protocol.

2.2. The model formulation

A PM model is constructed from the most basic elements of a tree (Früh and Kurth, 1999; Kumagai, 2001), as shown in Fig. 1b. This model treats the tree xylem as a porous medium, which obeys Darcy's law:

$$\hat{J} = -\hat{K} \frac{\partial \Psi}{\partial x}. \quad (1)$$

Here, \hat{J} is the water flux, \hat{K} the hydraulic conductivity and Ψ is the water potential consisting of two parts:

$$\Psi = \Phi + \rho gx; \quad (2)$$

the first term Φ is the hydrostatic pressure and the second term ρgx is the gravitational potential, ρ is the water density, g is the gravitational acceleration and x

is the vertical position along the tree. As is the case with a porous medium, loss of conductivity due to reduced moisture (or pressure) is empirically determined by vulnerability curves (Sperry and Tyree, 1990; Sperry et al., 1998; Ewers et al., 2000). A simplified vulnerability curve is a Weibull function:

$$\hat{K} = \hat{K}_{\max} e^{-\left(\frac{-\Phi}{d}\right)^{c_2}}, \quad (3)$$

where \hat{K}_{\max} is the maximum conductivity, c_2 and d are fitting parameters.

The storage of water within the tree is represented by its xylem moisture content $\theta(x, t)$ bounded by θ_{sat} (i.e., storage is saturated) and 0 (i.e., the storage is completely drained), and the hydraulic capacitance is defined as:

$$c = \frac{\partial \theta}{\partial \Phi}. \quad (4)$$

The relation between Φ and θ is determined by an empirical retention curve, which is usually fitted by a logarithm curve (Kumagai, 2001). However, the logarithm relation does not correctly reflect the extreme conditions: since $\Phi = -\infty$ is not practical on the field, it may not be an issue that the logarithm relation gives $\theta = -\infty$ under this condition, but the other extreme, $\theta = \theta_{\text{sat}}$ under $\Phi = 0$, is well achievable. The logarithm relation results in $\theta = +\infty$ under this condition, which is not only unphysical but can also cause serious problems for our model. Therefore, we adopt the following relation:

$$\frac{\theta}{\theta_{\text{sat}}} = \left(\frac{\Phi_0}{\Phi_0 - \Phi} \right)^P, \quad (5)$$

where Φ_0 and P are empirical parameters. This relation is characteristically similar to the logarithm one in a moderate potential range and exactly matches both extreme conditions.

By modifying the continuity equation to include a sink term $S(x, t)$ for transpiration, the dynamics of xylem moisture content $\theta(x, t)$ follows the conservation law:

$$\frac{\partial(A(x)\theta(x, t))}{\partial t} + \frac{\partial \hat{J}}{\partial x} = S(x, t), \quad (6)$$

where $A(x)$ is the cross section area of the tree. The sink term can be characterized by:

$$S(x, t) = -l(x)E(x, t), \quad (7)$$

where $l(x)$ is the local leaf area density (i.e., leaf area per unit stem length) and $E(x, t)$ is the transpiration flux density.

Combining Eq. (1), (2), (4), (6) and (7), the prognostic Partial Differential Equation (PDE) for $\theta(x, t)$ reduces to:

$$\frac{\partial\theta(x, t)}{\partial t} - \frac{1}{A(x)} \frac{\partial}{\partial x} [\rho g A(x) K(\theta)] - \frac{1}{A(x)} \frac{\partial}{\partial x} \left[A(x) \frac{K(\theta)}{c(\theta)} \frac{\partial\theta(x, t)}{\partial x} \right] = -\frac{l(x)}{A(x)} E(x, t), \quad (8)$$

where $K(\theta)$ defined as $\hat{K}/A(x)$ is the xylem hydraulic conductance. Both $K(\theta)$ and $c(\theta)$ are material properties of trees and thus affected by the moisture content. The material properties may have spatial inhomogeneity within a real tree, which can introduce an explicit spatial dependence to K and c . For simplicity, we ignore this spatial inhomogeneity.

2.3. Calculating the sap flux

Although Eq. (8) computes $\theta(x, t)$, the observed quantity in field experiments is the sap flux $J(x, t)$, defined as $\hat{J}(x, t)/A(x)$. To compute $J(x, t)$ from $\theta(x, t)$, we note that (1), (2), (4) and (5) imply an explicit formula:

$$J(x, t) = - \left[\rho g K(\theta) + \frac{K(\theta)}{c(\theta)} \frac{\partial\theta(x, t)}{\partial x} \right]. \quad (9)$$

Note that conductance K appears in Eq. (9) instead of conductivity \hat{K} since $J(x, t)$ is $\hat{J}(x, t)$ divided by $A(x)$.

2.4. Determining the boundary conditions

The boundary conditions consist of two parts: *roots* and *crowns*.

The root boundary condition (i.e., lower boundary condition) assumes that the soil moisture content remains nearly constant at time scales comparable to diurnal VPD changes. Therefore, the xylem moisture content at tree base also remains relatively constant. For simplicity and without loss of generality, let us assume the base xylem moisture content is near saturation, i.e.,

$$\frac{\theta(x=0, t)}{\theta_{\text{sat}}} = \frac{\theta_S}{\theta_{S\text{sat}}} \cong 1. \quad (10)$$

This assumption places the tree under moist condition. Employing the model under dryer conditions requires the explicit measurements of the base xylem moisture content, which becomes the *effective saturated xylem moisture content* for the model. This measured quantity replaces the real saturated xylem moisture content and acts exactly the same as θ_{sat} as in the near saturation condition. If the relation between xylem moisture of the tree base and soil moisture can be formulated during a wet-dry period, the variation of the soil moisture content can then be referred to govern this lower boundary condition of the model.

For the crown boundary condition (i.e., upper boundary condition), we note that the transpiration flux density $E(x, t)$ is already incorporated in Eq. (8) so that the treetop is treated as no-flux boundary condition (i.e., no leakage)

$$J(x=1, t) = - \left[\rho g K(\theta) + \frac{K(\theta)}{c(\theta)} \frac{\partial\theta(x, t)}{\partial x} \right]_{x=1} = 0. \quad (11)$$

2.5. Non-dimensionalizing the equations

The PDE (Eq. (8)) and the boundary conditions (Eqs. (10) and (11)) contain parameters and variables with physical units. First, we apply a standard procedure used in analyzing non-linear physics models, that of non-dimensionalization. By removing the unit-dependence from the model, we (1) write the equations in a more general form instead of only for a specific tree, (2) combine various parameters into dimensionless compound parameters which determine the dynamics of the model and thus (3) simplify the symbols of the analysis. Although the model is only applied to the experimental data from a single tree, we hope that it serves as a useful method for later data analysis. This procedure is standard and common because it reveals the underline formula of a model; models which share the same dimensionless form exhibit the same analytical behaviors. Therefore, non-dimensionalizing the model before performing the linear stability analysis eliminates the need to repeat the analysis for each tree and is useful in future research.

The premise of non-dimensionalization is to rescale the state variable θ as well as the spatial and temporal coordinates x and t so that the units are eliminated

Table 1
List of parameter values and physical constants used for model simulation in this study: parameter values are also listed and the model output variables are labeled as calculated

Symbol	Value in SI unit		Dimensionless value
A_0	0.0131	H^2	2.90×10^{-4}
E	Calculated	$H\theta_{\text{sat}}\eta^{-1}$	Calculated
H	6.7	H	1
J	Calculated	$H\theta_{\text{sat}}\eta^{-1}$	Calculated
K_{max}	5.47×10^{-8}	η	1.52×10^{-11}
P	400	1	400
T	1.20×10^{-4}	η^{-1}	0.433
c_2	3.5	1	3.5
d	6.8×10^6	$H^2\theta_{\text{sat}}\eta^{-2}$	3.41×10^9
g	9.8	$H\eta^{-2}$	1.89×10^7
\mathcal{E}	Calculated	$H^3\theta_{\text{sat}}\eta^{-1}$	Calculated
Φ_0	2.87×10^9	$H^2\theta_{\text{sat}}\eta^{-2}$	1.44×10^{12}
α	0.425	H^{-1}	2.85
κ	6.82×10^{-4}	$H^2\eta^{-1}$	5.46×10^{-2}
θ_{sat}	573.5	θ_{sat}	1
ρ	10^3	θ_{sat}	1.74
τ	3600	η	1

The value with units can be computed by multiplying the dimensionless values with the non-dimensionalization factors.

from the model and the solution does not depend on any specific dimension, thereby revealing canonical properties of water flow in trees. In order to do so, we may substitute the follows into the model equations:

- $x = Hx'$, where H is the total height of the tree;
- $\theta = \theta_{\text{sat}}\theta'$, where θ_{sat} is the saturated moisture content;
- $t = \eta t'$, where η is usually a character time or a time scale of the dynamics.

The primed variables are the dimensionless version of the unprimed ones. By combining the three scaling constants H , θ_{sat} and η , we can non-dimensionalize the other model parameters. The complete dimensionless variables and parameters of the model are listed in Table 1.

By replacing the dimensional (unprimed) variable with dimensionless (primed) ones and then dropping the primes to clear the expression, the resultant dimensionless PDE takes the following form:

$$\frac{\partial\theta(x, t)}{\partial t} - \frac{1}{A(x)} \frac{\partial}{\partial x} [\rho g A(x) K(\theta)] - \frac{1}{A(x)} \frac{\partial}{\partial x} \left[A(x) \frac{K(\theta)}{c(\theta)} \frac{\partial\theta(x, t)}{\partial x} \right] = -\frac{l(x)}{A(x)} E(x, t), \tag{12}$$

where x and θ are dimensionless and both simply range from 0 to 1; the functional forms of the dimensionless vulnerability curve and retention curve are still identical to Eqs. (3) and (5), respectively, except that the arguments and parameters become dimensionless while the dimensionless capacitance is defined as in Eq. (4). The dimensionless boundary conditions are also obtained:

$$\theta(x = 0, t) = 1 \quad (\text{root}), \tag{13}$$

$$\rho g K(\theta) + \frac{K(\theta)}{c(\theta)} \frac{\partial\theta(x, t)}{\partial x} \Big|_{x=1} = 0 \quad (\text{crown}). \tag{14}$$

When the results are presented, the units of choice (for example, the SI units) can be restored to the calculated quantities.

2.6. Linear stability analysis

Linear stability analysis, which is widely used to analyze the models of non-linear systems (Nicolis, 1995, pp. 71–93; Greenside and Cross, 2002, pp. 65–122), has three primary steps: (1) solving for the steady state solution, (2) perturbing the steady state solution and (3) applying the boundary conditions.

The tree approaches a steady state condition at night when transpiration (i.e., the driving force of the model) is zero. For $E(x, t) = 0$, the steady state solution (i.e., $\partial\theta/\partial t = 0$) of Eq. (12) can be analytically derived:

$$\theta_0(x) = \left(\frac{\Phi_0}{\Phi_0 + \rho g x} \right)^P. \tag{15}$$

For most of the cases when the porous media is relatively rigid, which is the case of the tree hydraulic system, $P|\rho g x| \ll |\Phi_0|$; thus,

$$\theta_0(x) = 1, \tag{16}$$

i.e., the tree is nearly saturated at night when soil moisture is high. When using the model under non-saturated soil moisture conditions Eq. (16) means that the xylem moisture content is near its effective saturation point set by the dryer condition.

Nighttime measured sap flux decays toward zero while the shape of its vertical profile appears unchanged as shown in Fig. 2, which suggests a relaxation mechanism. Therefore, the relaxation phenomena can be captured with linear stability analysis. We per-

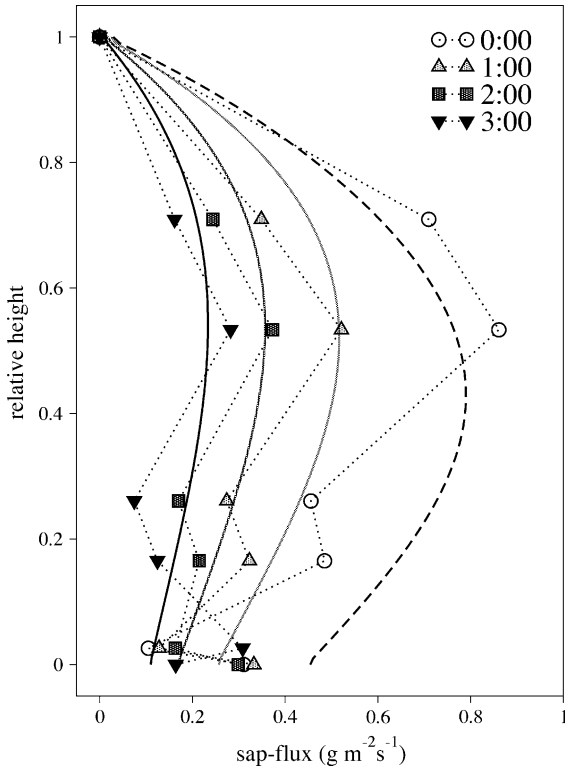


Fig. 2. Comparison of the vertical profile of sap flux between field measurements (symbols and dotted lines) and model simulation (dashed or solid lines) for hourly runs beginning midnight until 3:00. In both measurements and simulated results, sap flux preserves the shape of the eigenfunction in space as it relaxes in time.

turb the steady state solution by assuming:

$$\theta(x, t) \cong \theta_0(x) - \tilde{\theta}(x, t) \quad \text{where} \quad \tilde{\theta}(x, t) \ll \theta_0(x), \tag{17}$$

and then substitute it into Eq. (8) with $E(x, t) = 0$. Using the approximation shown in Eq. (16) to the linear order, $\tilde{\theta}(x, t)$ satisfies:

$$\begin{aligned} \frac{\partial \tilde{\theta}(x, t)}{\partial t} &= \left(\frac{k}{c}\right)_{\theta=1} \frac{\partial^2 \tilde{\theta}(x, t)}{\partial x^2} \\ &+ \left(\frac{(dA(x)/dx)}{A(x)} - \rho g \frac{c_2}{d} \left(\frac{\Phi}{d}\right)^{c_2-1} \Big|_{\theta=1}\right) \\ &\times \left(\frac{K}{c}\right)_{\theta=1} \frac{\partial \tilde{\theta}(x, t)}{\partial x}, \end{aligned} \tag{18}$$

where K and c are both evaluated at $\theta = 1$.

Next, using separation of variables and eigenfunction expansion, $\tilde{\theta}(x, t)$ can be expressed as:

$$\tilde{\theta}(x, t) = \sum_i e^{-T_i t} b_i(x),$$

where T_i is the time constant of the spatial eigenfunction $b_i(x)$. Assuming T_j is the smallest time constant among T_i s, the corresponding spatial eigenfunction $b_j(x)$ dominates the other $b_i(x)$ s as t increases. Therefore, $\tilde{\theta}(x, t)$ converges toward the asymptotic solution:

$$\tilde{\theta}(x, t) \cong e^{-T_j t} b_j(x).$$

For simplicity, we drop the subscript j and write $\tilde{\theta}(x, t)$ as:

$$\tilde{\theta}(x, t) = e^{-Tt} b(x). \tag{19}$$

Substituting Eq. (19) back into Eq. (18), it can be shown that $b(x)$ must satisfy:

$$\begin{aligned} \frac{d^2 b(x)}{dx^2} &+ \left(\frac{(dA(x)/dx)}{A(x)} - \rho g \frac{c_2}{d} \left(\frac{\Phi}{d}\right)^{c_2-1} \Big|_{\theta=1}\right) \\ &\times \frac{db(x)}{dx} + \frac{T}{(K/c)_{\theta=1}} b(x) = 0. \end{aligned} \tag{20}$$

For analytical tractability, let us assume the cross section area of the tree trunk tapers exponentially, i.e.,

$$A(x) = A_0 e^{-\alpha x}, \tag{21}$$

where A_0 is the cross section area at the tree base and α is the taper rate. This assumption is generally a reasonable approximation. The most notable consequence of this assumption is that it simplifies Eq. (20) in that

$$\frac{(dA(x)/dx)}{A(x)} = -\alpha.$$

Let

$$\kappa \equiv \left(\frac{K}{c}\right)_{\theta=1} = \frac{\Phi_0 k_{\max}}{P}, \tag{22}$$

and note that if $c_2 > 1$, which is true for typical vulnerability curves:

$$\left(\frac{\Phi}{d}\right)^{c_2-1}\Big|_{\theta=1} = 0. \tag{23}$$

Then, $b(x)$ can be *analytically* solved:

$$b(x) = b_0 e^{\alpha x} \sin \left[\left(\frac{\alpha}{2} \sqrt{\frac{4T}{\kappa\alpha^2} - 1} \right) x \right] + b_1 e^{\alpha x} \cos \left[\left(\frac{\alpha}{2} \sqrt{\frac{4T}{\kappa\alpha^2} - 1} \right) x \right]. \tag{24}$$

As a result, the perturbation function satisfies:

$$\tilde{\theta}(x, t) = b_0 e^{-Tt+\alpha x} \sin \left[\left(\frac{\alpha}{2} \sqrt{\frac{4T}{\kappa\alpha^2} - 1} \right) x \right] + b_1 e^{-Tt+\alpha x} \cos \left[\left(\frac{\alpha}{2} \sqrt{\frac{4T}{\kappa\alpha^2} - 1} \right) x \right], \tag{25}$$

while $\theta(x, t) = \theta_0 - \tilde{\theta}(x, t) \cong 1 - \tilde{\theta}(x, t)$.

Eq. (25) is the general functional form for the perturbation near the steady state solution of the PM model (Eq. (8)). However, not all functions that match the general form are solutions for a specific problem because the boundary conditions have to be satisfied. Only a subset of the functions will meet the requirement.

The root boundary condition leads to:

$$b_1 = 0,$$

in Eqs. (24) and (25) and thus, reduces the perturbation function to:

$$\tilde{\theta}(x, t) = b_0 e^{-Tt+\alpha x} \sin \left[\left(\frac{\alpha}{2} \sqrt{\frac{4T}{\kappa\alpha^2} - 1} \right) x \right]. \tag{26}$$

Furthermore, the crown boundary condition can be rewritten as:

$$\frac{\partial\theta(x, t)}{\partial x} \Big|_{x=1} = -\rho g c(\theta) \Big|_{x=1}.$$

Substituting $\theta(x, t) = \theta_0(x) - \tilde{\theta}(x, t)$ into the above equation to the linear order, we obtain:

$$\frac{\partial\tilde{\theta}(x, t)}{\partial x} \Big|_{x=1} = -\rho g \frac{dc(\theta)}{d\theta} \Big|_{\theta=\theta_0} \tilde{\theta}(x, t) \Big|_{x=1};$$

then, using the expression in Eq. (26) for $\tilde{\theta}$,

$$b_0 e^{-Tt+\alpha} \left(\frac{\alpha}{2} \sqrt{\frac{4T}{\kappa\alpha^2} - 1} \right) \cos \left(\frac{\alpha}{2} \sqrt{\frac{4T}{\kappa\alpha^2} - 1} \right) + b_0 e^{-Tt+\alpha} \alpha \sin \left(\frac{\alpha}{2} \sqrt{\frac{4T}{\kappa\alpha^2} - 1} \right) = -\rho g \frac{dc(\theta)}{d\theta} \Big|_{\theta=\theta_0 \cong 1} \cdot b_0 e^{-Tt+\alpha} \times \sin \left(\frac{\alpha}{2} \sqrt{\frac{4T}{\kappa\alpha^2} - 1} \right). \tag{27}$$

Since c is defined by Eq. (4) and θ is given by Eq. (5),

$$\frac{dc(\theta)}{d\theta} \Big|_{\theta=\theta_0 \cong 1} = \frac{P+1}{\Phi_0},$$

Thus,

$$\rho g \frac{dc(\theta)}{d\theta} \Big|_{\theta=\theta_0 \cong 1} = \rho g \frac{P+1}{\Phi_0} << 1$$

and then Eq. (27) can be simplified to:

$$\tan \left(\frac{\alpha}{2} \sqrt{\frac{4T}{\kappa\alpha^2} - 1} \right) \cong -\frac{1}{\alpha} \left(\frac{\alpha}{2} \sqrt{\frac{4T}{\kappa\alpha^2} - 1} \right). \tag{28}$$

Hence, for α estimated from the trunk diameter profile and T obtained from the relaxation time series, Eq. (28) can be used to numerically solve for κ . The solution is a discrete spectrum; nevertheless, the dominant eigenfunction during the night is the slowest decaying mode corresponding to the largest value of κ . The physical meaning of κ is the inverse of RC constant in saturated state according to Eq. (22).

2.7. Parameterization of the model

Before numerical results are presented, we discuss the parameter values and the units. Because the numerical simulation of models can be done more systematically with the non-dimensionalized version, the dimensionless parameters are presented along with their values in SI units in Table 1. Non-dimensionalization starts with rescaling the state variable and the coordinates; while we have one state variable (θ) and two coordinates (x, t), three

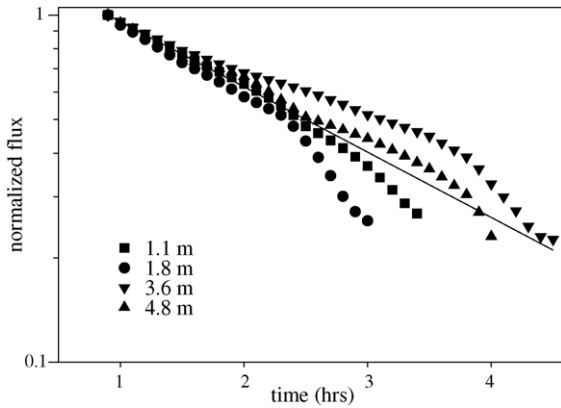


Fig. 3. Nighttime sap flux versus time on a log scale from 0:30 to 4:30 at four heights. To leading order, an average relaxation constant T can be computed from the slope of the regression analysis.

rescaling constants are necessary and sufficient: (1) the total height of the tree $H=6.7$ m, which rescales x to 0–1, (2) the saturated xylem moisture content $\theta_{\text{sat}}=0.574 \text{ m}^3 \text{ H}_2\text{O m}^{-3}$ stem, which rescales θ to 0–1 and (3) a suitable time constant η , which is usually chosen to normalize a parameter or to project the problem onto a time scale comparable to the characteristic time of the dynamics. We use $\eta=1 \text{ h}=3600 \text{ s}$ because the sap flux variation primarily responds to the diurnal pattern of environmental factors and thus, the dynamics is conveniently described on an hourly basis.

The other parameters and variables can further be non-dimensionalized based on these three constants. The central piece of the parameterization is the evaluation of the saturated inverse RC constant (κ), defined by Eq. (22). The process starts with the determination of the relaxation time constant T of the nighttime sap flux and the taper rate α of the stem cross section area. T is evaluated by regressing the logarithm of the nighttime sap flux with time, as shown in Fig. 3. The deviation of the relaxation curves from each other is likely due to spatial inhomogeneity among the measurement points, as well as the experimental noise where sap flux is low. (Note that the plot is on a log scale where a small noise is magnified at lower values.) Despite the deviations, the common relaxation tendency among the measurement points is strong, showing that the relaxation behavior is a relatively dominant phenomenon. Thus, the relaxation behavior is the first-order approximation for the nighttime dynamics. The relaxation constant T

obtained from the figure is $1.20 \times 10^{-4} \text{ s}^{-1}$ in SI units. On the other hand, the exponential taper function (Eq. (21)) matches the cross section area measurements of the tree in the Norway spruce experiment, as shown in Fig. 4a. Therefore, α is directly fitted as 0.425 m^{-1} in SI units. Once T and α are known, Eq. (28) can be numerically solved to obtain $\kappa=6.82 \times 10^{-4} \text{ m}^2 \text{ s}^{-1}$.

While the data is not available to parameterize the vulnerability curve (Eq. (3)) and the retention curve (Eq. (5)), the choice of the P – Φ_0 – K_{max} combination is not unique for a given κ . In the Section 4, we point out that the model results are similar for different combinations because the most important parameter in the model is the lump sum parameter $\kappa=\Phi_0 K_{\text{max}} P^{-1}$, rather than the three individual parameters. Using an approximated description, we adopt $P=400$, $\Phi_0=2870 \text{ MPa}$ and thus $K_{\text{max}}=5.47 \times 10^{-8} \text{ s}$ in SI units.

One may refer to Appendix A for the details of the parameterization as well as the non-dimensionalization of the entire model. The final results are listed in Table 1.

2.8. Calculating the crown transpiration rate

With the parameter values determined, the next step is estimating the daytime transpiration from the measured sap flux. While the model, Eq. (8), calculates the sap flux from a given transpiration rate, our objective is aligned with the inverse problem: evaluating the transpiration rate from the measured sap flux time series.

In this subsection, three methods for generating transpiration from measured sap flux are presented. The first method is the prevailing method and serves as the “baseline” or “reference” method to assess the descriptive and predictive skills of the porous media model. The second method is a full simulation of the porous-media PDE and requires several iterations to back-calculate the transpiration rate from the sap flux data. The third method is derived from simplifications to the PDE. Unlike the full PDE method, we simply integrate an ODE one time; therefore, this method is more computationally efficient.

The prevailing method for calculating transpiration rate from sap flux time series is called cross-correlation (CC) method. In principle, it has two steps: mass conservation and storage effects. The first step uses the

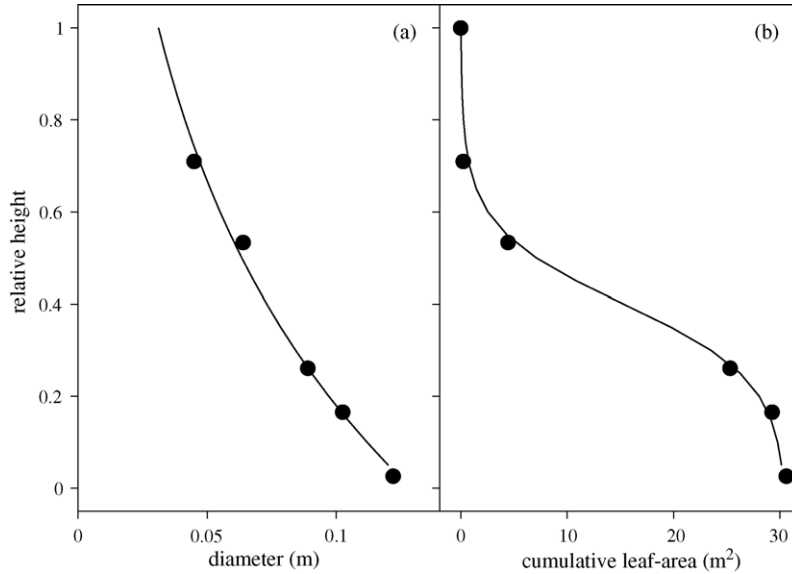


Fig. 4. Vertical profile of (a) diameter and (b) cumulative leaf area of the study *Picea abies* tree. The data for diameter are fitted with: diameter = $0.129 \times \exp(-1.42 \times \text{relative height})$. The data for cumulative leaf area are approximated with: cumulative leaf area = $15.3 \times (1 - \tanh(6 \times \text{relative height} - 2.4))$.

principle of mass conservation and assumes no water storage within a tree. As a result, the sap flux, $J(x, t)$, through the tree stem must transpire into the atmosphere somewhere along the path. Thus, we can subtract the sap flow at a higher level in the stem from the flow at a lower level and obtain the total amount of transpired water between the two levels. Knowing the trunk cross section area, $A(x)$, and the leaf area density $l(x)$, we can further calculate $E(x, t)$ by:

$$[A(x_L)J(x_L, t) - A(x_H)J(x_H, t)] = l \left(\frac{x_L + x_H}{2} \right) (x_H - x_L) E \left(\frac{x_L + x_H}{2}, t \right), \quad (29)$$

where x_L is a lower level and x_H is a higher level along the tree.

The second step considers the storage effects. The water storage inside the tree empties in the morning and refills in the evening, thus sap flux is delayed relative to transpiration. Noting that the actual $E(x, t)$ is often synchronized with VPD and/or incoming R_g , the measured sap flux is commonly shifted backward in time relative to the time series of both VPD and R_g , until the best correlation coefficient is found. The lag with the highest correlation to either VPD or R_g

is assumed to account for the storage-related delay (hereafter referred to as ‘time lag’). The shifted sap flux is treated as a representation of $E(x, t)$ (Phillips et al., 1999; Schäfer et al., 2000). The advantage of this method is simplicity and ease of implementation. However, there are some disadvantages when considering the effect of water storage by simple time shifts; the storage not only delays the sap flux response to environmental driving variables, but also modulates it. The consequence is that the increased flow of morning sap flux is less dramatic than the actual transpiration rate, and correspondingly, there exists a relaxing tail in evening sap flux as VPD or R_g and actual transpiration approach zero. This extra tail is discarded and leads to a net loss of water when calculating transpiration rates using this method.

For the PM method, we note that if the actual $E(x, t)$ is known, the PDE in Eq. (8) can be numerically integrated over space and time by applying the boundary conditions, Eqs. (10) and (11). Once $\theta(x, t)$ is computed, $J(x, t)$ can be calculated using Eq. (9):

$$J(x, t) = - \left[\rho g K(\theta) + \frac{K(\theta)}{c(\theta)} \frac{\partial \theta(x, t)}{\partial x} \right].$$

In the field, $J(x, t)$, not $E(x, t)$ is measured. Therefore, a method that inverts from sap flux to transpiration is of interest. We consider an iterative method:

1. Provide an initial guess for $E(x, t)$.
2. Integrate the PDE and calculate the corresponding $J(x, t)$.
3. Compare the calculated $J(x, t)$ with the experimentally measured sap flux data $J_e(x, t)$ and evaluate the difference between $J(x, t)$ and $J_e(x, t)$ (i.e., $\Delta J(x, t) = J_e(x, t) - J(x, t)$).
4. Assume the entire difference $\Delta J(x, t)$ contributes to the difference between the assumed transpiration rate $E(x, t)$ and the actual one $E_a(x, t)$.
5. Convert $\Delta J(x, t)$ into the difference in transpiration rate: $\Delta E(x, t) = \Delta J(x, t) A(x)/(l(x) \Delta x)$, where Δx is the spatial grid size in numerical simulation.
6. Calculate the corrected transpiration rate: $E_{\text{new}}(x, t) = E(x, t) + \Delta E(x, t)$.
7. Employing $E_{\text{new}}(x, t)$ as the new initial guess for $E(x, t)$, repeat steps 1–6 until the difference between the experimental and the simulated data reaches its minimum. Further iterations magnify the experimental noise and move the simulated results away from the experimental data.

This procedure requires several iterations (17 for this case study) before the best agreement between simulation and data is achieved. The full PDE simulation should provide accurate results. However, full PDE simulations are time consuming for some applications, which motivated us to attempt to simplify the calculations. We decompose the full PDE model into simpler ordinary differential equations (ODE) and propose a quicker method to calculate transpiration rate from sap flux data while still preserving the advantages of the PDE porous media model.

The quantity measured in the field is $J(x, t)$. We can compute θ from J data by notifying that Eq. (9) can be rewritten as

$$\frac{\partial \theta(x, t)}{\partial x} = - \frac{J(x, t) + \rho g K(\theta)}{\frac{K(\theta)}{c(\theta)}}, \quad (30)$$

which is an ODE for any given time t . Knowing that $\theta(x=0, t) = \theta_{\text{sat}}$ is the lower boundary condition, we integrate $\theta(x, t)$ from $x=0$ to H to obtain $\theta(x, t)$ as a function of x at time t . Since the resolution of $J(x, t)$ is usually low, we interpolate between the measurement

heights to integrate Eq. (30) over finer spatial grids. One thing to note is that the interpolations should be done on the sap flow data, i.e., $A(x)J(x, t)$, rather than the sap flux ($J(x, t)$) in order to preserve the total mass.

Because $J(x, t)$ is measured as a time series, we integrate Eq. (30) at each different time and reconstruct $\theta(x, t)$ as a time series. After $\theta(x, t)$ is obtained, we substitute it back into PDE Eq. (8):

$$\frac{\partial \theta(x, t)}{\partial t} - \frac{1}{A(x)} \frac{\partial}{\partial x} [\rho g A(x) K(\theta, x)] - \frac{1}{A(x)} \frac{\partial}{\partial x} \left[A(x) \frac{K(\theta, x)}{c(\theta, x)} \frac{\partial \theta(x, t)}{\partial x} \right] = - \frac{l(x)}{A(x)} E(x, t) \quad (31)$$

and simply discretize space and time to calculate $E(x, t)$. This procedure eliminates the need for iteration.

3. Results

In this study, the primary forcing variable is sap flux, which is readily measured in field experiments. Night-time sap flux measurements are used to obtain storage properties of trees, which in-turn allow computing day-time transpiration rates.

3.1. Model verification using the nighttime sap flux results

All the model parameters can be directly measured or independently estimated from the nighttime sap flux data where linear stability analysis applies. Agreement between measured and modeled sap flux during nighttime can provide the necessary confidence that the model represents the key mechanisms responsible for plant hydrodynamics. By setting $E(x, t) = 0$, the PDE of the PM model can be numerically integrated to obtain the nighttime sap flux. The results of the nighttime model simulations compare well with the measurements made in the Norway spruce tree (Fig. 2). The measured sap flux data is very close to the simulated results despite experimental noise and possible spatial inhomogeneity within the tree system (data point number (N) = 28, correlation (r^2) = 0.84, maximum value (Max) = $0.86 \text{ g m}^{-2} \text{ s}^{-1}$, root mean square error (RMSE) = $0.13 \text{ g m}^{-2} \text{ s}^{-1}$ in Fig. 2; N = 49, r^2 = 0.83, Max = $2.54 \text{ g m}^{-2} \text{ s}^{-1}$, RMSE = $0.33 \text{ g m}^{-2} \text{ s}^{-1}$ for the

entire nighttime data). Even more interesting is that the analytical form of the nighttime sap flux can be derived by substituting the perturbation eigenfunction (Eq. (26)) of the moisture content,

$$\begin{aligned}\theta(x, t) &= \theta_{\text{sat}} - \tilde{\theta}(x, t) \\ &= \theta_{\text{sat}} - b_0 e^{-Tt+\alpha x} \sin \left[\left(\frac{\alpha}{2} \sqrt{\frac{4T}{\kappa\alpha^2} - 1} \right) x \right],\end{aligned}$$

into the sap flux calculation in Eq. (9). This suggests that the analytical form of nighttime flux is well defined.

3.2. Daytime transpiration rate calculation

The transpiration rate was back-calculated based on experimentally measured sap flux data by inverting the porous media PDE that computes the sap flux from a given transpiration rate. The straightforward method is to fully simulate and iterate the PDE. The non-zero transpiration rate is the driving force of the model during daytime. For height-dependent simulation of transpiration rate, the leaf area density $l(x)$ on the right hand side of the PDE (Eq. (8)) is needed in order to properly scale sap flux to transpiration rate. This $l(x)$ (Fig. 4b) was measured through a destructive harvest of the tree at the conclusion of the experiment (Phillips et al., 2004).

The results of the full PDE simulation (dashed lines in Fig. 5, left panels) are compared with those from the CC method (dotted lines). For the CC method, the time series of sap flux is shifted relative to VPD and R_g forward and backward in time steps equal to the measurements resolution until the highest correlation coefficient is reached. This analysis shows higher maximum correlation coefficient with R_g ($r^2 = 0.85$, averaged over the five crown zones) than with VPD ($r^2 = 0.75$). The R_g -lagged sap flux produces transpiration patterns that begin at a similar time to that calculated with the PDE method, but rise more slowly, do not display the same dynamics during the day, and trail off later into the night in all five crown zones. We note that the transpiration rate at the top and bottom crown sections are very high relative to the three mid-sections. This is the result of having very little leaf area in both sections, making small errors in flow, measured or simulated, produce high rates of transpiration.

Because the full PDE simulation is time-consuming, we derive an alternative ODE method. The solid lines on the left hand side of Fig. 5 are the results of this ODE method, and follow the overall pattern of the full PDE simulations, but reflect greater and more rapid fluctuations. The greater fluctuations calculated with ODE relative to the fluctuations with PDE generate large differences in transpiration at any point in time. Although the ODE method can be integrated much more quickly, the huge fluctuation resulting from the measurement noise is a disadvantage. The lack of robustness to the noise is evident because after integrating the ODE (Eq. (30)) over x to obtain $\theta(x, t)$ (which is contaminated by noise in the sap flux), noise in the time series amplifies when the term $\partial\theta(x, t)/\partial t$ in Eq. (31) is computed.

The high-frequency noise generated by the ODE method can be reduced through filtering. The simplest filter is a moving average and can be implemented by taking the average at each time step with its adjacent data points (i.e., high-frequency filtering). The solid lines on the right hand side of Fig. 5 show the results after employing such a filter, using a 5-point moving average. The filtered results of the alternative ODE method are much smoother and close to the full PDE simulation ($N = 1200$, $r^2 = 0.90$).

The transpiration rates from the two PM methods and the CC method drop below zero at certain points (Fig. 5). This drop is due to the unavoidable measurement noise in the sap flux time series. The measurements with least noise occur between the measurement points $Z/H = 0.27$, just below the height in which significant amount of foliage can be found (Fig. 4b), and 0.54. The sap flux data are obtained from the measured temperature gradient between a heated and unheated probe (Granier et al., 1996). Thus, the noise introduced in the lower measurement points originates from thermal fluctuation of the ground, while the noise at higher measurement points generates negative transpiration only when the sap flux approaches zero. Due to the tapering of the cross section of the trunk (Fig. 4a), the total sap flow (sap flux times cross section area) is much smaller at the highest measurement point, and therefore, the experimental noise produces “negative” transpiration more often than at mid-tree height positions.

To confirm that the inverse problem is solved properly, we compute the daytime sap flux using the PDE-simulated transpiration as the boundary conditions. The obtained sap flux compares very well with

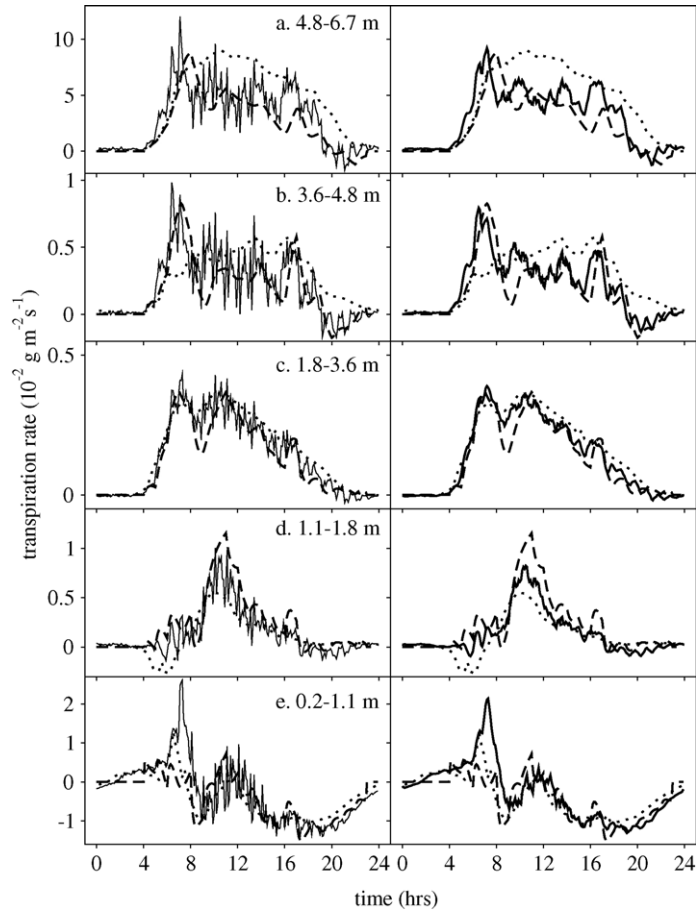


Fig. 5. Height-dependent transpiration rate (i.e., transpiration rate between consecutive heights) obtained by lagging sap flux based on cross-correlation (CC; dotted lines) analysis with global radiation and the simulated with two porous media methods, one based on partial differential equations (PDE; dashed lines) and one on ordinary differential equations (ODE; solid lines) at five height intervals in the tree (left hand side panels). The right hand side panels show the same data, except that the results from the ODE are filtered based on 5-point moving average, with each point representing 0.1 h.

the experimental measurements ($N=119$, $r^2=0.98$, $\text{Max}=18.00 \text{ g m}^{-2} \text{ s}^{-1}$, $\text{RSME}=1.02 \text{ g m}^{-2} \text{ s}^{-1}$). Two typical snapshots of the comparison between the vertically explicit sap flux simulation and measurement show a good agreement along the entire tree stem (Fig. 6).

4. Discussion

The intent of the proposed porous media model is to simulate water flux in trees by isolating the xylem hydraulic system from other complex organs (e.g.,

stomata, root–soil matrix), rather than to simulate the flux in every organ of the tree. For this reason, the soil moisture content is treated as a constant within the time scale of the problem, and the morphology and the spatial inhomogeneity are left for future studies. Moreover, because the focus of this model is on internal hydraulic control of water flux dynamics, dynamical changes in stomatal conductance (Tardieu and Davies, 1993; Friend, 1995; Leuning, 1995; Oren et al., 1999; Eamus and Shanahan, 2002; Dewar, 2002) are not included here. In principle, a submodel of stomatal conductance could be straightforwardly coupled with this PM model by providing an independent transpiration time series.

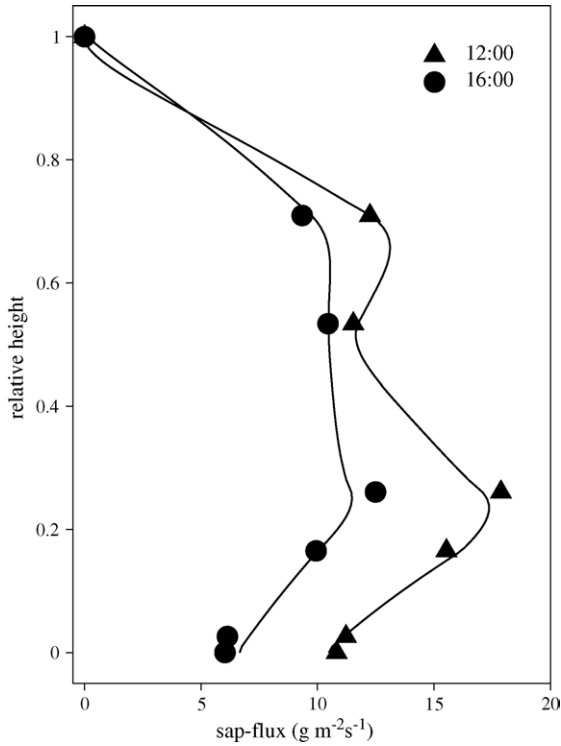


Fig. 6. Comparison of the vertical profile of sap flux between field measurements (symbols) and model simulation (solid lines) for hourly runs at midday and 16:00.

Isolating the xylem hydraulic system from stomatal conductance and from variation in forcing variables leads to a logical separation between nighttime (no transpiration) and daytime dynamics. The primary difference between nighttime and daytime sap flux is its relaxation behavior, as shown in Figs. 2 and 3. Because stomata close at night, the hydraulic system of a tree is isolated from any change in canopy environment and relaxes toward a steady state. The saturated RC constant, κ^{-1} , is determined when the relaxation time constant T is fitted. Therefore, it is not surprising that the relaxation rate of the experiment data is similar to that of the model simulation (Fig. 2). On one hand, the vertical agreement between the experimentally measured data and analytically predicted eigenfunction (Fig. 2) shows that the complexity is greatly reduced by isolating the system from the environment at nighttime. The agreement serves as an independent verification of the PM model for the hydraulic system of trees and

suggests nighttime data as a good starting point for modeling the plant hydraulic system.

Analysis of nighttime sap flux data (Fig. 3) can be utilized to evaluate the saturated RC constant, κ^{-1} . Assuming that moisture content is not far from saturation, κ^{-1} is essentially R times C and provides a systematic method to calculate the RC constant for the electrical circuit analogue model. The analysis shows that the parameter of the stem taper function appears in the formula that evaluates the relaxation time constant (Eq. (28)). To our knowledge, the effect of the stem taper has not been previously considered in quantifying the time lag in sap flux. If we assume that the tree is a uniform rod, the relaxation time constant of our model reduces to $(2\pi H^{-1})^2 (Kc^{-1})_{\theta} = 1$, which is equivalent to $(RC)^{-1}$ for the circuit analogy. Thus, the stem taper modifies the time lag from the perfect RC constant predicted by a simplified RC circuit model. Additionally, the stem taper also distorts the vertical profile of sap flux from a simpler sinusoidal function predicted by the uniform-rod assumption. Thus, our analysis provides another explanation for the difference between RC -predicted and actual sap flow data shown in Phillips et al. (1997) where the RC model does not consider the effect of stem taper on sap flow dynamics. This also means that if the taper of a tree is other than exponential, it is necessary to revisit the nighttime data analysis in order to derive a new formulation for κ .

Phillips et al. (2004) utilize the perturbed (i.e., step changes in VPD) sap flux data on the same Norway spruce tree to study the applications of RC circuit models. The time constant, i.e., RC , is estimated from the lag of the morning rise in the slope of the sap flux behind that of the ecosystem latent heat flux, and was 106 min. Using their formula and the κ from our PM simulation, the equivalent RC constant for this tapering spruce tree is ~ 72 min. Although there is some difference between these two estimates of the RC constant, the variation of C can range 3–27-fold within moderate range of xylem water potential (Holbrook, 1995, pp. 151–174). More importantly, the smaller RC constant of our model is expected, given the analysis of a ramp-function forced RC circuit (Phillips et al., 2004). Direct integration of the RC circuit equation readily shows that the lag between sap flux and latent heat flux is the time interval on which the capacitance current (i.e., storage flux) damps out. Although this time interval is not well defined, it should be longer than the “true” RC time

constant where the capacitance current damps to 36% of its original value. Therefore, the 72 min obtained from the PM model may reflect the “true” RC number of this tree.

On the other hand, the saturated RC constant (κ^{-1}), as a lump-sum parameter, is the primary governing parameter of the PM model (see Section 2.7). Coupled with Eq. (9), the model computes the sap flux while being driven by the transpiration rate. Because the transpiration rate and the sap flux are physically equivalent quantities (only through different cross section areas), this mechanism makes both the moisture content θ and the water potential Φ transient variables. This is a key advantage over previous PM models because θ and Φ are difficult to obtain in a field experiment. There is a parallel situation in an RC circuit driven by a current source. While further specifying R and C can uniquely determine the voltage and the charges in the capacitors, the lump-sum RC constant alone is enough to determine the dynamics of the electrical current. This advantage allows our model to produce reasonably good results even though the vulnerability curve (specifying the conductance) and the retention curve (specifying the capacitance) are not readily measured in the experiment, and we have to use empirical curves instead. Consequently, one has to be cautious about the calculated θ and Φ as well; although they combine to correctly evaluate the sap flux, each of θ and Φ is only qualitatively meaningful. They can be made quantitatively meaningful if either the retention curve or the xylem conductivity is obtained from the experiment.

During the daytime, stomata open and the xylem hydraulic system is no longer isolated from its environment. Both the full PDE simulation and the ODE alternative method produce a transpiration rate that begins at about the same time as the shifted “transpiration” produced by lagging sap flux based on the CC method (Fig. 5). This indicates that the time lag is already accounted for by the PM methods. Although the time lag is easier to correct by artificial shifting, the choice between correlating sap flux with VPD or R_g may not be conclusive because they both can affect its dynamics. Therefore, shifting sap flux to the better correlation of the two may not reflect the actual time lag between sap flux and transpiration rate, especially in situations in which VPD and R_g are not highly synchronized. Moreover, as stated earlier, the CC method cannot restore transpiration rate from the attenuated response in sap

flux because, unlike PM and RC models, the method does not simulate the storage mechanism. The reduced response in sap flux produces a relaxation tail when VPD and transpiration drop to zero. The CC method cannot redistribute the water within the tail, which is typically discarded, causing a net loss of water (Phillips and Oren, 1998; Ewers and Oren, 2000).

Two indicators that the PM model more accurately describes the physics of the water flow than the CC method are time lag and attenuation effect. Since the storage mechanism is embedded in the two PM methods, its effects are dealt with realistically, resulting in reasonable approximation of sap flow dynamics inside a tree. As stated earlier that the transpiration rates calculated by both PM methods rise at the same time as the results obtained by the CC method (Fig. 5), suggesting that they estimate the same time lag. Furthermore, the PM methods give a higher rate for morning transpiration and a more rapid decay for evening transpiration than the CC method. Thus, PM methods better address the attenuation effects, which are not addressed by the CC method. On the other hand, the mass-conserving formulation of the PM model ensures no net water loss. Table 2 summarizes the calculated total daily transpiration at each measurement height in Fig. 5. Since R_g is the primary environment factor that affects the transpiration in this specific case, the results of the CC method are obtained by discarding the data between 21:00 and 3:30 when R_g is close to zero, as described in Section 2.8. The table shows that the ODE method nicely recaptures the discarded water. However, the PDE method does not perform as well as the ODE method in this specific case. It is likely due to a sudden drop of the global radiation around 8:00 which is followed by a drop in the sap flux thereafter, as shown in Fig. 7(top). Because the PDE simulation is searching for continuous and differentiable solutions, which can hardly match such a sudden change, the method produces an anomaly around 8:00 (Fig. 5). Because the data fitting must find the best match for the entire range, this local anomaly contributes to a significant water loss. This phenomenon shows that the ODE method, which tolerates big fluctuations, has an advantage over the PDE method when dealing with noisy data sets. Nevertheless, the ODE method is derived from the PDE, so we believe the PDE method should perform better given a less noisy data set, which can be achieved by averaging over a larger sample size.

Table 2

Daily transpiration which is calculated by integrating the curves in Fig. 5 through an entire day and multiplying the leaf areas at five vertical sections; the results of three different methods are shown for comparison (CC method with and without data cutoff are both listed):

Vertical position (m)	CC method (without cut) (g)	CC method (g)	PDE method (g)	ODE method (g)
a. 4.8–6.7	856.67	710.42	565.06	658.46
b. 3.6–4.8	967.07	795.15	845.65	847.39
c. 1.8–3.6	2857.9200	2583.06	2517.33	2867.91
d. 1.1–1.8	350.48	310.45	808.43	513.70
e. 0.2–1.1	–398.62	–219.32	–266.66	–266.01
Total	4633.53	4179.76	4469.80	4621.44

We tested the model on a conifer tree, but the formulation is sufficiently general that with proper parameterization the model should be applicable to broadleaf species despite differences in xylem structure. This generality is valid because the model uses averaged macroscopic velocities rather than the micro-

scopic velocities within an individual xylem element. That is, as long as the macroscopic flow through a group of vessels follows Darcy’s law, then the general porous media ansatz should hold. We obtain reasonable results for a conifer tree while neglecting hysteresis. Since hysteresis is known to be more of an issue for small pores (e.g. conifer xylem) than large pores (e.g., vessels in broadleaf trees), we expect the PM model to readily adapt to broadleaf species.

There are two other potential problems of applying the model to broadleaf species: One is that in some species, stem cross section area changes with transpiration, which can impact the storage flux term (Zweifel et al., 2001; Zweifel and Hasler, 2001). However, this change must be compared to sources of water loss in the continuity equation. Recall from Eqs. (6) and (7) that

$$\frac{\partial(A(x)\theta(x, t))}{\partial t} + \frac{\partial \hat{J}}{\partial x} = -l(x)E(x, t);$$

hence, if

$$\theta(x, t) \frac{\partial A(x, t)}{\partial t} \ll A(x, t) \frac{\partial \theta(x, t)}{\partial t}$$

the change in stem cross section area has negligible effect on the model. Furthermore, if the change in cross sectional area with transpiration is restricted mostly to the bark (e.g., Zweifel et al., 2000), then the entire formulation must be made separately for xylem and bark. Our intention is to derive a formulation that is physically based, replacing the empirical formulation of the RC circuit, yet retaining some simplicity in the treatment of the tree.

The other potential problem is that some broadleaf species and even some conifers can have some nighttime transpiration (Oren et al., 2001; Snyder et

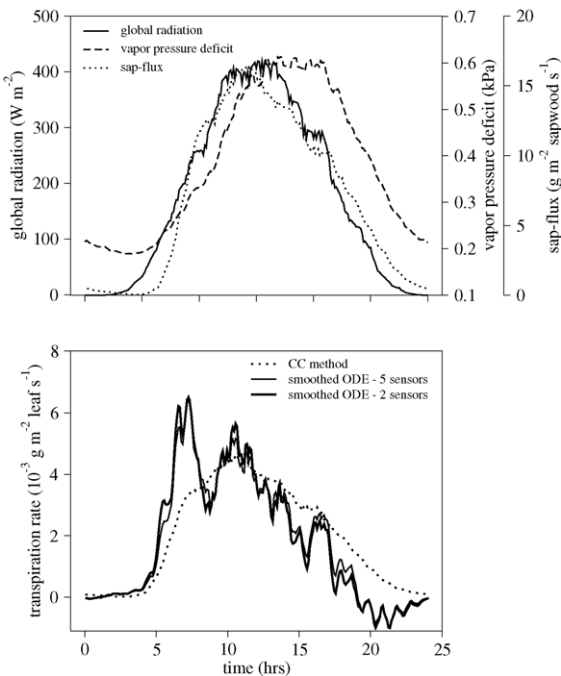


Fig. 7. Ensemble average over the experiment period of diurnal sap flux, global radiation and vapor pressure deficit showing a close similarity in the patterns of the two former variables (top). After lagging sapflux to better match global radiation, sapflux was scaled to average tree transpiration and compared to the simulated transpiration based on the ordinary differential equations (ODE; filtered based on 5-point moving average) using five measurement heights below and within the crown, or using two heights below the canopy.

al., 2003), which affects the estimation of κ . We can quantitatively estimate this effect by adding a small amount of transpiration ε to the right hand side of Eq. (18). This inhomogeneous equation results in an underestimation of κ , or equivalently an overestimation of $c(\theta)$ on the order of ε/E , the ratio of the nighttime transpiration to the daytime transpiration, which is usually under 10%. Even when the nighttime transpiration is relatively large, a no-transpiration period (e.g., continuous rain events, or low VPD conditions) can provide sufficient data for model parameterization.

Our model can be improved and made more versatile in a number of ways. For example, Aumann and Ford (2002a) recently composed a more complete PM model for the hydraulic system. In addition to the wetting phase (i.e., the sap fluid), their model calculates the movement of the de-wetting phase (i.e., the water vapor) as well. Because the presence of water vapor is associated with reduction of xylem conductivity due to cavitation, the function of the vulnerability curves are not needed in their model. However, in order to obtain the dynamics of the de-wetting phase, the model parameterization is done at the tracheid scale (Aumann and Ford, 2002b), and thus, the parameters are not readily obtainable via field measurements. Although their model is experimentally challenging for quantitative verification and may require simplifying assumption for application, it is more realistic than ours in that it accounts for the inability of the xylem to immediately recover upon re-wetting the conductivity lost during water discharge. Inclusion of the de-wetting phase may represent an improvement for our PM model. However, our aim is to produce a model that can readily serve to study the water flow at tree rather than tracheid scale and thus, help in determining the ecological variables related to transpiration rate, such as stomatal conductance and CO₂ flux, also at tree scale.

On the other hand, there are several potential improvements to our model that may increase its versatility. This includes explicit treatment of spatial inhomogeneity of conductance and capacitance, and branching structure. With such improvements, the model can be used to study the more fluctuating dynamics of sap flux, frequently observed in branches and reflected in ecosystem-level latent heat flux (Oren et al., 1998; Phillips et al., 1999).

4.1. Applications

In order to overcome the sensor noise, our analysis was done with a 17-day ensemble mean of sap flux. Although temporal averaging can be used to reduce noise, such averaging if done over a too long of a period may mask changing parameter values with changing environmental conditions. For example, the time constant for nighttime stem recharge can increase with decreasing soil moisture (Phillips et al., 1996). Installing a sufficient number of sensors at each height can also reduce the noise in the flux measurements (Oren et al., 1998), thus producing a spatially averaged flux, while preserving the temporal dynamics.

We show that flux measurements in multiple points within and below the crown can account for the role of tree hydraulics in regulating gas exchange. However, for broader, ecological scale studies aiming at quantifying biosphere–atmosphere exchange of mass and energy, such intensive measurements are impractical and probably unfeasible. Loustau et al. (1996) showed that measurements of sap flux below the crown and lower in the stem can be used to quantify the quantity of water discharged and recharged in stems, and combined with additional data estimated transpiration from sap flux using an RC model (Loustau et al., 1998).

Although the spatial accuracy of the sap flux data obviously increases as more probes are used to measure at different heights, an advantage of our PM model, which we now demonstrate, is that only two measurements at different heights are required if the bulk transpiration rate of the tree is the desired quantity. The most ideal choice for these two measurement points is one near the tree base and the other one near the bottom of the crown. However, due to thermal gradients, measurements too near to the soil tend to be unreliable, and due to the influence of nearby branches, measurements too near to crowns with large branches may generate large spatial inhomogeneity (Loustau et al., 1996). Thus, sensors are best placed about 1 m from each.

We re-analyzed the flow obtained at 1.1 and 1.8 m above ground to simulate transpiration based on measurements made at two heights. We assessed the performance of the PM model to reproduce the bulk transpiration based on two measurement heights by comparing with the transpiration simulated based on all available five measurement heights. We used the ODE method so the test is made with the more practical of the two PM

methods, and smoothed out the high frequency noise using a moving average. Note that in general the averaging process must be conducted within a time scale much smaller than the characteristic time scale of the simulated dynamic phenomena. For example, if the averaging is taken within the time scale comparable to the time lag of the sap flux, the simulated transpiration might become smeared and lagged behind the actual transpiration.

The ensemble mean diurnal pattern of R_g showed a simple bell-shaped curve, closely followed by that of the sap flux (Fig. 7(top)). The diurnal pattern of VPD was a little more attenuated and displaced later in the day. The bulk transpiration is almost the same whether all five or only two measurement heights are used (Fig. 7(bottom)); $N=240$, $r^2=0.99$, $\text{Max}=0.65 \text{ g m}^{-2} \text{ s}^{-1}$, $\text{RMSE}=0.026 \text{ g m}^{-2} \text{ s}^{-1}$). As was observed in the analysis of the height-dependent transpiration (Fig. 5), the time-lagged transpiration based on the CC method rose at a lower rate in the morning, showed a strongly attenuated signal, and trailed late into the night. We conclude that, to the extent that transpiration was simulated well by the PM method based on the five measurement heights, only two measurement heights are necessary to obtain equally good simulations.

Theoretically, this conclusion can be shown by multiplying Eq. (8) with $A(x)$ and then integrating it over x . After applying the boundary conditions,

$$\frac{\partial \Theta(t)}{\partial t} + \rho g A_0 K_{\max} + \frac{\Phi_0 K_{\max}}{P} A_0 \left. \frac{\partial \theta(x, t)}{\partial x} \right|_{x=0} = -\mathcal{E}(t),$$

where

$$\Theta(t) = \int_0^H A(x) \theta(x, t) dx;$$

$$\mathcal{E}(t) = \int_0^H l(x) E(x, t) dx.$$

Therefore, the factors that affect the calculated total transpiration $\mathcal{E}(t)$ are (1) the total moisture content $\Theta(t)$ and (2) the slope of the moisture content $\partial \theta(x, t)/\partial x$ at $x=0$. They are both obtained via Eq. (30) using $J(x, t)$ interpolated or extrapolated from the measured data. As long as the process of interpolation and extrapolation well preserves the total mass, i.e., the total moisture

content, the results of the 2-point calculation are consistent with those of multiple-point calculations.

5. Conclusion

We develop a conifer hydraulic model using the porous media analogy and theoretically analyze the model to link its parameters to field observations. The separation of the nighttime data from the daytime data provides an isolated circumstance that allows us to verify the model independently. The nighttime analysis relates the time lag (i.e., the relaxation time constant) to the parameters of the retention and the vulnerability curves. Considering the current theoretical and experimental limitations, we propose that the model is most practically useful in translating measured sap flux data into transpiration rates. There are two primary advantages of this model over the CC method: (1) there is no need to shift the data to compensate the time lag because it has been physically corrected through the storage term; (2) there is no net water loss while converting the measured sap flux data into the transpiration rate because the entire water storage mechanism is resolved. The disadvantage is that the porous media model requires computation of a dynamic PDE. However, there exists an alternative ODE method, which is much simpler yet produces results close to those from the full PDE simulation. With transpiration rate calculated by the model in conjunction with VPD, bulk stomatal conductance can be inferred. Such estimates of bulk stomatal conductance from sap flux measurements have broad applications in ecological and hydrological sciences. For example, they can be used in field experiments at the whole plant or forest scale to assess the responds of mean tree or canopy stomatal conductance to anthropogenic perturbations such as elevated atmospheric CO_2 , added fertilization, or increases in ozone concentration, and to estimate biosphere–atmosphere exchanges of mass (CO_2 and H_2O) and energy Schäfer et al., 2003).

Acknowledgments

The authors gratefully acknowledge the support from the Center on Global Change at Duke University. Support was also provide by the National Sci-

ence Foundation (NSF) through NSF-EAR and NSF-DMS, and by the U.S. Department of Energy's Office of Science (BER), through the Southeast Regional Center (SERC) of the National Institute for Global Environmental Change (NIGEC) under Cooperative Agreement No. DE-FC03-90ER61010, and through the Terrestrial Carbon Processes Program (TCP). We are grateful to Prof. Sune Linder of the Swedish University of Agricultural Sciences for providing logistical support and use of experimental facilities at the Flakaliden Research Forest. YC and AB acknowledge support from the Army Research Office through Contract #DAAD19-02-1-0055 and the Office of Naval Research through Contract #N00014041 0078 and N00014041 0054.

Appendix A

In this appendix, we detail the parameterization and the non-dimensionalization of the model based on the three constants, H , θ_{sat} , and η^- , given in Section 2.7. First, sap flux is the quantity used to compare model simulation with experimental data. It can be made dimensionless by the factor $H\theta_{\text{sat}}\eta^{-1}$, and the translation between the flux in SI units and the dimensionless flux is: $H\theta_{\text{sat}}\eta^{-1} = 1068.94 \text{ g m}^{-2} \text{ s}^{-1}$.

Then we treat the physical constants, water density (ρ) and gravitational acceleration (g), which are both independent of trees. They can be non-dimensionalized as follows:

- $\rho = 10^3 \text{ kg m}^{-3} = 1.74368\theta_{\text{sat}}$;
- $g = 9.8 \text{ m s}^{-2} = 1.89 \times 10^7 H\eta^{-2}$.

The parameterization of T and α is described in Section 2.7. The dimensionless values of these two parameters are $T (=1.20 \times 10^{-4} \text{ s}^{-1}) = 0.433 \eta^{-1}$ and $\alpha (=0.425 \text{ m}^{-1}) = 2.85H^{-1}$, respectively. As T and α are known, we may solve Eq. (28) to find the smallest positive root (corresponding to the largest κ) of $\{\alpha\sqrt{[(4T\kappa^{-1}\alpha^{-1}) - 1]}\}/2$, which equals to $2.43 H^{-1}$ when $\alpha = 2.85H^{-1}$. Given $T = 0.433 \eta^{-1}$, $\kappa = 0.0546H^2\eta^{-1} (=6.82 \times 10^{-4} \text{ m}^2 \text{ s}^{-1})$.

While the data is not available to parameterize the retention curve in Eq. (5), we adopt an approximated description that P has to be large, making the slope steep near $\Phi = 0$, and choose Φ_0 so that θ can-

not dip below 70% at $\Phi = -2 \text{ MPa}$. At worst, it is still better than the general choice of constant capacitance (c) that allows a tree to have infinite storage capacity if a very large water potential difference is applied. We point out in the Discussion section that determination of the retention curve is not important to the results because of the transpiration-driving-sap-flux mechanism in the model. Consistent with this description, we choose a $P = 400$ (dimensionless already), and $\Phi_0 = 2870 \text{ MPa}$ (SI units) $= 1.44 \times 10^{12} H^2 \theta_{\text{sat}} \eta^{-2}$ (dimensionless units). With $\kappa = \Phi_0 K_{\text{max}} P^{-1}$ determined in the previous paragraph, the maximum conductance K_{max} can be calculated as $K_{\text{max}} = 1.52 \times 10^{-11} \eta$ (dimensionless units) $= 5.47 \times 10^{-8} \text{ s}$ (SI units).

To run the model, it is also necessary to obtain the fitting constants c_2 and d of the vulnerability curve. Linear stability analysis shows that, under the assumption that the moisture content is near the effective saturation at night, these two constants do not affect the dynamics of nighttime sap flux. However, it can affect daytime runs and needs to be quantified. The vulnerability curve was not measured in the 1996 experiment; therefore, we resorted to an estimate from the literature (Ewers et al., 2000) with $c_2 = 3.5$ (dimensionless already) while $d = 3.41 \times 10^9 H^2 \theta_{\text{sat}} \eta^{-2}$ (dimensionless units) $= 6.8 \text{ MPa}$ (conventional units). Although the numbers were obtained from loblolly pine (*Pinus taeda* L.), rather than Norway spruce, the effect is minimal on our simulation results because of the transpiration-driving-sap flux mechanism in the model.

Note that for the simplicity of formulation, the model simulations are done with dimensionless quantities and the results are converted to SI units for presentation. However, dimensional quantities can also be used for simulation, but the normalization constants must be restored to the formula. Therefore, Eq. (28) restores to:

$$\tan\left(\frac{\alpha}{2}\sqrt{\frac{4T}{\kappa\alpha^2} - 1} \cdot H\right) \cong -\frac{1}{\alpha}\left(\frac{\alpha}{2}\sqrt{\frac{4T}{\kappa\alpha^2} - 1}\right),$$

if H is not normalized to 1. Eq. (22) also restores to:

$$\kappa = \frac{\Phi_0 K_{\text{max}}}{H\theta_{\text{sat}} P}$$

for a non-normalized θ_{sat} .

References

- Aumann, C.A., Ford, E.D., 2002a. Modeling tree water flow as an unsaturated flow through a porous medium. *J. Theor. Biol.* 219, 415–429.
- Aumann, C.A., Ford, E.D., 2002b. Parameterizing a model of Douglas Fir water flow using a tracheid-level model. *J. Theor. Biol.* 219, 431–462.
- Baldocchi, D.D., Meyers, T., 1998. On using eco-physiological, micrometeorological and biogeochemical theory to evaluate carbon dioxide, water vapor and trace gas fluxes over vegetation: a perspective. *Agric. For. Meteorol.* 90, 1–25.
- Čermák, J., Cienciala, E., Kučera, J., Lindroth, A., Bednářová, E., 1995. Individual variation of sap flow rate in large pine and spruce trees and stand transpiration: a pilot study at the central NOPEX site. *J. Hydrol.* 168, 17–27.
- Cowan, I.R., 1965. Transport of water in the soil–plant–atmosphere system. *J. Appl. Ecol.* 2, 221–239.
- Cowan, I.R., 1972. Oscillations in stomatal conductance and plant functioning associated with stomatal conductance: observations and a model. *Planta* 106, 185–219.
- Cushing, J.M., Dennis, B., Desharnais, A., Costantino, R.F., 1996. An interdisciplinary approach to understanding nonlinear ecological dynamics. *Ecol. Modell.* 92, 111–119.
- Dewar, R.C., 2002. The Ball–Berry–Leuning and Tardieu–Davies stomatal models: synthesis and extension within a spatially aggregated picture of guard cell function. *Plant Cell Environ.* 25, 1383–1398.
- Eamus, D., Shanahan, S.T., 2002. A rate equation model of stomatal responses to vapour pressure deficit and drought. *BMC Ecol.* <http://www.biomedcentral.com/1472-6785/2/8>.
- Ewers, B.E., Oren, R., 2000. Analysis of assumptions and errors in the calculation of stomatal conductance from sap flux measurements. *Tree Physiol.* 20, 579–590.
- Ewers, B.E., Oren, R., Sperry, J.S., 2000. Influence of nutrient versus water supply on hydraulic architecture and water balance in *Pinus taeda*. *Plant Cell Environ.* 23, 1055–1066.
- Friend, A.D., 1995. PGEN: an integrated model of leaf photosynthesis, transpiration, and conductance. *Ecol. Modell.* 77, 233–255.
- Früh, T., Kurth, W., 1999. The hydraulic system of trees: theoretical framework and numerical simulation. *J. Theor. Biol.* 201, 251–270.
- Goldstein, G., Meinzer, F., Monasterio, M., 1984. The role of capacitance in the water balance of Andean giant rosette species. *Plant Cell Environ.* 7, 179–186.
- Goldstein, G., Andrade, J.L., Meinzer, F.C., Holbrook, N.M., Cavelier, J., Jackson, P., Celis, A., 1998. Stem water storage and diurnal patterns of water use in tropical forest canopy trees. *Plant Cell Environ.* 21, 397–406.
- Granier, A., 1985. Une nouvelle méthode pour la mesure de flux de sève brute dans le tronc des arbres. *Ann. Sci. For.* 42, 193–200.
- Granier, A., Biron, P., Breda, N., Pontailleur, J.-Y., Saugier, B., 1996. Transpiration of trees and forest stands: short and long-term monitoring using sapflow methods. *Glob. Change Biol.* 2, 265–274.
- Granier, A., Bobay, V., Gash, J.H.C., Gelpe, J., Saugier, B., Shuttleworth, W.J., 1990. Vapor flux density and transpiration rate comparisons in a stand of maritime pine (*Pinus pinaster* Ait.) in Les Andes Forest. *Agric. For. Meteorol.* 51, 309–319.
- Greenside, H.S., Cross, M.C., 2002. Pattern Formation and Dynamics of Non-equilibrium System. Cambridge University Press, 373 pp.
- Holbrook, N.M., 1995. Stem water storage. In: Gartner, B.L. (Ed.), *Plant Stems: Physiology and Functional Morphology*. Academic Press, p. 440.
- Hunt Jr., E.R., Nobel, P.S., 1987. Non-steady-state water flow for three desert perennials with different capacitances. *Aust. J. Plant Physiol.* 14, 363–375.
- Hunt Jr., E.R., Running, S.W., Federer, C.F., 1991. Extrapolating plant water-flow resistances and capacitances to regional scales. *Agric. For. Meteorol.* 54, 169–195.
- Jarvis, P.G., Edwards, W.R.N., Talbot, H., 1981. *Models of Crop Water Use. Mathematics and Plant Physiology*. Academic Press, London, 320 pp.
- Jones, H.G., 1992. *Plant and Microclimate*, second ed. Cambridge, 428 pp.
- Kumagai, T., 2001. Modeling water transportation and storage in sapwood—model development and validation. *Agric. For. Meteorol.* 109, 105–115.
- Lai, C.-T., Katul, G., Oren, R., Ellsworth, D., Schäfer, K., 2000. Modeling CO₂ and water vapor turbulent flux distributions within a forest canopy. *J. Geophys. Res.* 105, 26,333–26,351.
- Lang, A.R.G., Klepper, B., Cumming, M.J., 1969. Leaf water balance during oscillation of stomatal aperture. *Plant Physiol.* 44, 826–830.
- Leuning, R., 1995. A critical appraisal of a combined stomatal-photosynthesis model for C₃ plants. *Plant Cell Environ.* 18, 339–355.
- Loustau, D., Domec, J.-C., Bose, A., 1998. Interpreting the variations in xylem sap flux density within the trunk of maritime pine (*Pinus pinaster* Ait.): application of a model for calculating water flows at tree and stand levels. *Ann. Sci. For.* 55, 29–46.
- Loustau, D., Berbigier, P., Roumagnac, P., Arruda-Pacheco, C., David, J.S., Ferreira, M.I., Pereira, J.S., Tavares, R., 1996. Transpiration of a 64-year-old maritime pine stand in Portugal. *Oecologia* 107, 33–42.
- Marshall, D.C., 1958. Measurement of sap flow in conifers by heat transport. *Plant Physiol.* 33, 385–396.
- Nicolis, G., 1995. *Introduction to Nonlinear Science*. Cambridge University Press, 254 pp.
- Oren, R., Phillips, N., Katul, G., Ewers, B.E., Pataki, D.E., 1998. Scaling xylem sap flux and soil water balance and calculating variance: a method for partitioning water flux in forests. *Ann. Sci. For.* 55, 191–216.
- Oren, R., Sperry, J.S., Katul, G.G., Pataki, D.E., Ewers, B.E., Phillips, N., Schäfer, K.V.R., 1999. Survey and synthesis of intra- and interspecific variation in stomatal sensitivity to vapour pressure deficit. *Plant Cell Environ.* 22, 1515–1525.
- Oren, R., Sperry, J.S., Ewers, B.W., Pataki, D.E., Phillips, N., Mego-nigal, J.P., 2001. Sensitivity of mean canopy stomatal conductance to vapor pressure deficit in a flooded *Taxodium distichum* L. forest: hydraulic and non-hydraulic effects. *Oecologia* 126, 21–29.

- Patten, B.C., 1997. Synthesis of chaos and sustainability in a nonstationary linear dynamic model of the American black bear (*Ursus americanus* Pallas) in the Adirondack Mountains of New York. *Ecol. Modell.* 100, 11–42.
- Phillips, N., Oren, R., 1998. A comparison of daily representations of canopy conductance based on two conditional time-averaging methods and the dependence of daily conductance on environmental factors. *Ann. Sci. For.* 55, 217–235.
- Phillips, N.G., Oren, R., Licata, J., Linder, S., 2004. Time series diagnosis of tree hydraulic characteristics. *Tree Physiol.* 24, 879–890.
- Phillips, N., Oren, R., Zimmermann, R., 1996. Radial trends in xylem sap flow in non-, diffuse- and ring-porous species. *Plant Cell Environ.* 19, 983–990.
- Phillips, N., Bergh, J., Oren, R., Linder, S., 2001. Effects of nutrition and soil water availability on water use in a Norway spruce stand. *Tree Physiol.* 21, 851–860.
- Phillips, N., Nagchaudhuri, A., Oren, R., Katul, G., 1997. Time constant for water transport in loblolly pine trees estimated from time series of evaporative demand and stem sapflow. *Trees* 11 (7), 412–419.
- Phillips, N., Oren, R., Zimmermann, R., Wright, S.J., 1999. Temporal patterns of water flux in trees and lianas in a Panamanian moist forest. *Trees* 14, 116–123.
- Pielke, R.A., Schimel, D.S., Lee, T.J., Kittel, G.F., Zeng, X., 1993. Atmosphere-terrestrial ecosystem interactions: implications for coupled modeling. *Ecol. Modell.* 67, 5–18.
- Schäfer, K.V.R., Oren, R., Tenhunen, J.D., 2000. The effect of tree height on crown-level stomatal conductance. *Plant Cell Environ.* 23, 365–377.
- Schäfer, K.V.R., Oren, R., Ellsworth, D.S., Lai, C.-T., Herrick, J.D., Finzi, A.C., Richter, D.D., Katul, G.G., 2003. Exposure to an enriched CO₂ atmosphere alters carbon assimilation and allocation in a pine forest ecosystem. *Glob. Change Biol.* 9, 1378–1400.
- Schulte, P.J., Costa, D.G., 1996. A mathematical description of water flow through plant tissues. *J. Theor. Biol.* 180, 61–70.
- Slatyer, R.O., 1967. *Plant–Water Relationship*. Academic Press, New York, 366 pp.
- Snyder, K.A., Richards, J.H., Donovan, L.A., 2003. Night-time conductance in C₃ and C₄ species: do plants lose water at night? *J. Exp. Bot.* 54, 861–865.
- Sperry, J.S., Tyree, M.T., 1990. Water-stress-induced xylem embolism in 3 species of conifers. *Plant Cell Environ.* 13, 427–436.
- Sperry, J.S., Adler, F.R., Campbell, G.S., Comstock, J.P., 1998. Limitation of plant water use by rhizosphere and xylem conductance: result from model. *Plant Cell Environ.* 21, 347–359.
- Swanson, R.H., Whitfield, D.W.A., 1981. A numerical analysis of heat pulse velocity and theory. *J. Exp. Bot.* 32, 221–239.
- Tanaka, K., 2002. Multi-layer model of CO₂ exchange in a plant community coupled with the water budget of leaf surfaces. *Ecol. Modell.* 147, 85–104.
- Tardieu, F., Davies, W.J., 1993. Integration of hydraulic and chemical signalling in the control of stomatal conductance and water status of droughted plants. *Plant Cell Environ.* 16, 341–349.
- Verhoef, A., Allen, S.J., 2000. A SVAT scheme describing energy and CO₂ fluxes for multi-component vegetation: calibration and test for a Sahelian savannah. *Ecol. Modell.* 127, 245–267.
- Waring, R.H., Whitehead, D., Jarvis, P.G., 1979. The contribution of stored water to transpiration in Scots pine. *Plant Cell Environ.* 8, 613–622.
- Zhan, X., Xue, Y., Collatz, G.J., 2003. An analytical approach for estimating CO₂ and heat flux over the Amazonian region. *Ecol. Modell.* 162, 97–117.
- Zweifel, R., Hasler, R., 2001. Dynamics of water storage in mature subalpine *Picea abies*: temporal and spatial patterns of change in stem radius. *Tree Physiol.* 21, 561–569.
- Zweifel, R., Item, H., Hasler, R., 2000. Stem radius changes and their relation to stored water in stems of young Norway spruce trees. *Tree Struct. Funct.* 15, 50–57.
- Zweifel, R., Item, H., Hasler, R., 2001. Link between diurnal stem radius changes and tree water relations. *Tree Physiol.* 21, 869–877.